



Synthesis, characterization, and electrochemical properties of new water-soluble $Mn_{12}O_{12}(O_2CR)_{16}(H_2O)_4$ clusters

Naama Gluz & Galia Maayan

To cite this article: Naama Gluz & Galia Maayan (2018) Synthesis, characterization, and electrochemical properties of new water-soluble $Mn_{12}O_{12}(O_2CR)_{16}(H_2O)_4$ clusters, Journal of Coordination Chemistry, 71:11-13, 1971-1984, DOI: [10.1080/00958972.2018.1501033](https://doi.org/10.1080/00958972.2018.1501033)

To link to this article: <https://doi.org/10.1080/00958972.2018.1501033>



View supplementary material [↗](#)



Accepted author version posted online: 28 Jul 2018.
Published online: 19 Sep 2018.



Submit your article to this journal [↗](#)



Article views: 50



View Crossmark data [↗](#)

Synthesis, characterization, and electrochemical properties of new water-soluble $Mn_{12}O_{12}(O_2CR)_{16}(H_2O)_4$ clusters

Naama Gluz and Galia Maayan 

Schulich Faculty of Chemistry, Technion – Israel Institute of Technology, Haifa, Israel

ABSTRACT

We report our attempts to produce water-soluble Mn clusters of the type $[Mn_{12}O_{12}(O_2CR)_{16}(H_2O)_4]$ and the synthesis, spectroscopic, structural, and electrochemical characterization of the three new compounds that were obtained. Clusters **2**, **3**, and **4** were prepared via substitution of the acetate ligands in $[Mn_{12}O_{12}(O_2CMe)_{16}(H_2O)_4]$ (**1**) with either 3,4-diaminobenzoic acid, L-proline or L-ascorbic acid, respectively, which are all inexpensive and readily available. Clusters **2**, **3**, and **4** were characterized by elemental analysis, UV-Vis, and FTIR spectroscopies, XPS, MS, and XRD analysis, suggesting that the clusters retain their structure during the substitution reaction, albeit **4** was obtained partially substituted and reduced. Electrochemical measurements in acetate buffer at pH 6, including continuous cyclic voltammetry scans of the free ligands and of the clusters, imply that **4** is stable to the oxidation process, while in **2** the primary amine ligands are oxidized rapidly, leading to precipitation of the cluster. Overall, the voltammetric measurements support the spectroscopic-based proposed structures.

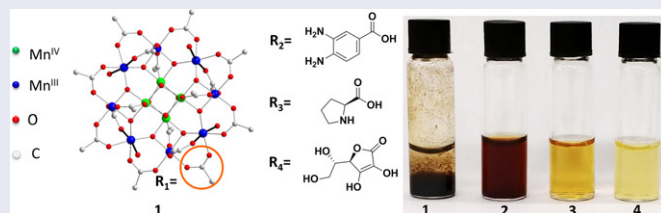
ARTICLE HISTORY

Received 15 February 2018
Accepted 9 July 2018

KEYWORDS

Manganese; oxidation;
electrocatalysis;
water-soluble

GRAPHICAL ABSTRACT



1. Introduction

Polynuclear manganese clusters, with the formula of $Mn_{12}O_{12}(O_2CR)_{16}(H_2O)_4$ ($R = Me, Et, Ph, etc., Mn_{12}$ clusters), have been investigated due to their ability to function as single-molecule magnets (SMMs) [1] and their relevance to bioinorganic chemistry [2].

CONTACT Galia Maayan  gm92@technion.ac.il  Schulich Faculty of Chemistry, Technion – Israel Institute of Technology, Haifa, Israel.

 Supplemental data for this article can be accessed at <https://doi.org/10.1080/00958972.2018.1501033>
Color versions of one or more of the figures in the article can be found online at www.tandfonline.com/gcoo.

© 2018 Informa UK Limited, trading as Taylor & Francis Group

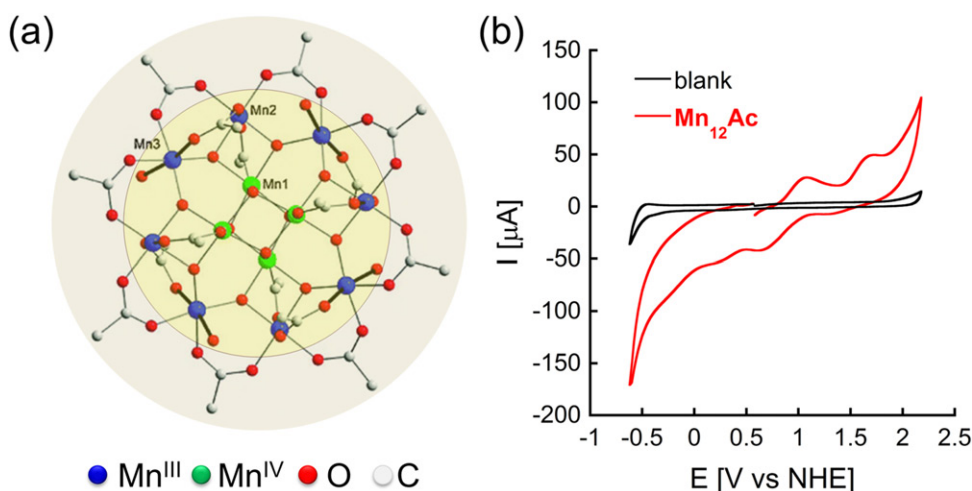
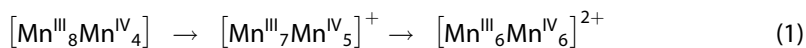


Figure 1. (a) The structure of $[\text{Mn}_{12}\text{O}_{12}(\text{O}_2\text{CMe})_{16}(\text{H}_2\text{O})_4]$ (**Mn₁₂Ac**, **1**) viewed along the molecular z axis; the thicker bonds identify the Mn^{III} Jahn–Teller elongation axes on which lie the four H_2O ligands. Hydrogens are omitted for clarity. (b) Cyclic voltammetry (CV) of 0.5 mM deoxygenated **1** at 100 mV/s in acetonitrile, scanning in the cathodic direction.

In the context of the latter, we note that the structure of these clusters resembles that of the oxygen-evolving complex (OEC) near photosystem II (PS II) of green plants and cyanobacteria, which is a Mn_4CaO_x species. The Mn_{12} acetate cluster (**Mn₁₂Ac**, **1**), for example, is composed of an inorganic core of 12 manganese ions held together by μ -oxo-bridges, surrounded by an organic shell of sixteen bridging carboxylate ligands and four labile water molecules (Figure 1a). The inorganic core consists of a $[\text{Mn}^{\text{IV}}_4\text{O}_4]$ cubane, connected by triply bridging oxygen ions to a nonplanar ring of eight Mn^{III} ions. Fourfold symmetry divides the eight outer Mn^{III} ions into two groups of four ions each, marked in Figure 1a as Mn2 and Mn3 [1]. These structural features allow for its rich redox chemistry and relatively high oxidation potentials. The cyclic voltammetry (CV) of **1**, for example (Figure 1b), exhibits four reversible one-electron processes, two oxidations at $E_p = 1.18$ and 1.44 V and two reductions at 0.35 and 0.56 V (vs. NHE; E_p is the peak potential). Previous studies describing the reduction processes of several Mn_{12} clusters have confirmed their one-electron nature by isolation of $[\text{Mn}_{12}]^{n-}$ ($n = 1-3$) salts, including crystallographic characterization of the $n = 1$ and 2 examples, which also showed the reductions to occur at outer Mn^{III} ions to give Mn^{II} [3]. Extension to the oxidations shown in Figure 1b confirms that these are also one-electron processes, which we assign to the oxidation of Mn^{III} ions (Equation (1)).



Cluster **1** is available in high yield from a one-step comproportionation reaction of Mn^{II} acetate and KMnO_4 in aqueous acetic acid [4]. Derivatives of this cluster having different R groups can be prepared from **1** by carboxylate substitution reactions, a well-studied and widely employed procedure in Mn_{12} chemistry (Equation (2)) where the substitution is being driven to completion by excess carboxylic acid with a greater acidity than acetic acid ($\text{pK}_a = 4.76$ at 25 °C).

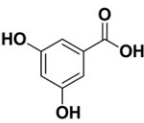
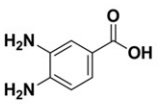
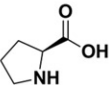
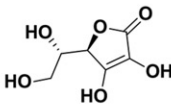
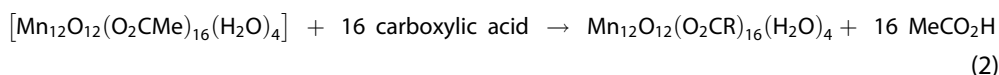
	Previous work	This work		
				
		dabH	proH	ascH
Water solubility at 25°C (g/L)	51	57.5	162	400 (at 40°C)
pKa (COOH)	4.04	3.49	1.95	4.10

Figure 2. Structure and relevant chemical properties of polar carboxylic acid ligands 3,4-diaminobenzoic acid (dabH), L-proline (proH) and L-ascorbic acid (ascH) used in this research, in comparison with the previously used ligand 3,5-dihydroxybenzoic acid.



Mn_{12} clusters have several desired properties, which make them attractive complexes for bioinorganic studies toward catalytic applications [1, 5]: (i) they all contain high oxidation state manganese ions (8Mn^{III} , 4Mn^{IV}), (ii) they display multiple one-electron redox processes (see Figure 1b for the cyclic voltammetry of **1**), whose exact values can be tuned by the choice of carboxylate R group, (iii) they have four water-binding sites that could facilitate water oxidation catalysis, and (iv) their structures resemble the CaMn_4O_5 oxygen-evolving complex in PSII, having the shared motif of $\text{Mn}^{\text{IV}}\text{-O-Mn}^{\text{III}}\text{-H}_2\text{O}$, which is essential for water oxidation. In addition, their synthesis is simple and green, involving inexpensive and abundant building blocks, and they are stable under normal aerobic conditions. Mn_{12} clusters are typically insoluble in water; those that do dissolve hydrolyze rapidly to insoluble Mn oxide/hydroxides. The insolubility and/or instability in water limit their utility for the applications mentioned above and specifically as potential water oxidation catalysts. One way to overcome the hydrolysis problem is to introduce carboxylate ligands that will enable water solubility and stability of the newly generated clusters.

Recently, we described the use of 3,5-dihydroxybenzoic acid as a ligand that is both bulky and hydrophilic for the synthesis of the Mn_{12} derivative **Mn₁₂DH**, which is both soluble and stable in water. We further demonstrated that **Mn₁₂DH** is a stable homogeneous water oxidation electrocatalyst operating at pH 6 with an exceptionally low overpotential of only 334 mV [6]. Following this discovery, we are now interested in exploring the use of other water-soluble carboxylate ligands with pKa of their carboxylic acid lower than that of **1** (4.76) as potential substituents for the organic shell of Mn_{12} acetate (see Equation (1)). Initially we chose three such ligands, 3,4-diaminobenzoic acid (dabH), L-proline (proH), and L-ascorbic acid (ascH), which are all inexpensive and readily available and incorporate a variety of types and number of hydrophilic groups (Figure 2). In this article, we describe our attempts to use these

ligands for preparation of new water-soluble Mn_{12} clusters. We demonstrate that while the displacements of acetate ligands by either dab or pro were successful, producing the corresponding Mn_{12} clusters, which show high solubility in water, the reaction with asch did not lead to the desired Mn_{12} cluster. All three products were characterized by spectroscopic analyses and their electrochemical properties in aqueous acetate buffer at pH 6 were investigated.

2. Experimental

2.1. Materials

Manganese(II) acetate tetrahydrate was purchased from Acros Organics. Potassium permanganate ($KMnO_4$) was purchased from Fisher chemicals. Water (HPLC grade), acetonitrile, 3,4-diaminobenzoic acid, and L-proline were purchased from Sigma Aldrich. L-Ascorbic acid was purchased from Alfa Aesar. Acetic acid, ethanolamine, methanol, ethanol, and acetone were purchased from Gadot chemicals. Reagents and solvents were used without purification.

2.2. Equipment

Elemental analyses (C, H, N or C, H, N, and O) were performed on a "Thermo-Scientific Flash 2000 elemental organic analyzer". Overall, three measurements were performed for each examined cluster. FTIR spectra ($400\text{--}4000\text{ cm}^{-1}$) were recorded on an "Agilent Cary 630" FTIR spectrometer, equipped with a diamond attenuated total reflection (ATR) instrument, allowing direct measurement with no sample preparation. UV-Vis spectroscopy measurements ($200\text{--}800\text{ nm}$) were performed on an "Agilent Cary 60" spectrometer at $25\text{ }^\circ\text{C}$ using a 1 cm path length quartz cell. X-ray Photoelectron Spectroscopy (XPS) was performed in the Solid-State Institute at the Technion, on a Thermo-VG SIGMA probe XPS spectrometer. Inductively coupled plasma (ICP) measurements were performed using a "Thermo-Scientific iCAP 6000" ICP-OES analyzer. The wavelength used for the detection of Mn was 257.6 nm . The sample contained a solution of 500 ppm **4** in HPLC grade water. MS analysis was performed on a Thermo-Scientific LCQ Fleet Ion-Trap Mass Spectrometer. Powder XRD measurements were performed in the Wolfson center for interface science at the Faculty of Science and Materials Engineering, Technion, on a Rigaku SmartLab 9 kW X-ray diffractometer utilizing $Cu\ \alpha$ radiation ($\lambda = 1.541\ \text{\AA}$). Measurement conditions: PB mode, 45 kV, 150 mA, step size: 0.01, speed: 2 deg/min., 2θ range: 0° to 60° . Cyclic voltammetry (CV) was conducted at room temperature using a 563 model "IVIUMSTAT.XRe" potentiostat/galvanostat. CV measurements were conducted in a standard three-electrode cell assembly consisting of a glassy carbon electrode as the working electrode, Pt mesh as the counter (auxiliary) electrode, and a Ag/AgCl/3M KCl reference electrode ($+210\text{ mV}$ vs. NHE). The CVs were typically recorded at a scan rate of 100 mV/s , Estep of 10 mV and sensitivity of 0.1 mA/V . No IR compensation was employed. The potential was measured versus the Ag/AgCl reference electrode and converted to versus NHE by using $E(\text{NHE}) = E(\text{Ag/AgCl}) + 0.21\text{ V}$. Deoxygenation was accomplished by bubbling N_2 through the solutions for 5 min.

2.3. Synthesis

2.3.1. Synthesis of $Mn_{12}O_{12}(O_2CCH_3)_{16}(H_2O)_4$ (1)

To a stirred solution of $Mn(O_2CMe)_2 \cdot 4H_2O$ (4.00 g, 16.3 mmol) in 60% v/v acetic acid in water (15 mL), a solution of $KMnO_4$ (1.0 g, 6.33 mmol) in 60% v/v acetic acid in water (25 mL) was added. The resulting dark brown solution was filtered and the filtrate was left undisturbed in an open flask for 2 days at room temperature. The resulting black crystals of $1 \cdot 2MeCO_2H \cdot 4H_2O$ were collected by filtration, washed with acetone until the washing solution became colorless, and dried in vacuum. Yield: 50%. IR (KBr pellet): 3598(w), 1709(w), 1588(m), 1559(m), 1521(m), 1451(s), 1388(s), 1334(m), 1256(w), 1023(w), 714(m), 675(m), 640(m), 609(m), 563(w), 507(w), 517(w), 410(m) cm^{-1} . Powder XRD, 2θ values of selected peaks: 7.19, 8.73 (100% intensity), 13.45, 14.26, 16.02, 17.58, 19.87, 22.31, 24.39, 30.05, 32.33, 42.30 and 54.14°.

2.3.2. Synthesis of $Mn_{12}O_{12}(O_2CC_6H_3(NH_2)_2)_{16}(H_2O)_4$ (2)

To a stirred solution of $1 \cdot 2MeCO_2H \cdot 4H_2O$ (0.25 g, 0.12 mmol) in acetonitrile (40 mL), solid 3,4-diaminobenzoic acid (0.73 g, 4.8 mmol) was added. Acetone (40 mL) was then added and the solution was stirred for 48 h, and the color changed slightly from dark brown to reddish-brown. The resulting brown precipitate was collected by filtration, washed with acetonitrile (5 mL), acetone (3×5 mL) and diethyl ether (3×5 mL), and dried in vacuum. Yield: 23%. The solid was analyzed as $[Mn_{12}O_{12}(O_2CC_6H_3(NH_2)_2)_{16}(H_2O)_4] \cdot 11H_2O \cdot 3MeCN$. Anal. Calcd for $C_{151}H_{195}N_{35}Mn_{12}O_{59}$: C, 44.196; H, 4.789; N, 11.946%. Found: C, 44.23; H, 4.42; N, 12.05%. FTIR: $\nu = 715\text{--}500$ (m, several Mn-O), 690–820 (m, substituted benzene Ar-N-H) 1300–1900 (s, several C=O), 1600–1400 (s, aromatic C=C), 1260–1440 (s, primary N-H deformations), 3280–3460 (m, stretching mode of N-H of primary amine) cm^{-1} . MS (ESI-MS) m/z: Calcd (for $[Mn_{12}O_{12}(O_2CC_6H_3(NH_2)_2)_{16}(H_2O)_4] \cdot 11H_2O \cdot 3MeCN$): 4103.04; Found: 3484.2 ($[Mn_{12}O_{12}(O_2CC_6H_3(NH_2)_2)_{16}(H_2O)_4] \cdot 8H_2O$). Powder XRD, 2θ values of selected peaks: 8.05, 8.84 (100% intensity), 11.53, 13.04, 16.14, 17.65, 19.25, 21.54, 25.64, 29.73, 31.52, 42.53, 49.4, 54.09°.

2.3.3. Synthesis of $Mn_{12}O_{12}(O_2CC_4H_8N)_{16}(H_2O)_4$ (3)

To a stirred solution of $1 \cdot 2MeCO_2H \cdot 4H_2O$ (0.25 g, 0.12 mmol) in acetonitrile (40 mL), solid L-proline (0.56 g, 4.83 mmol) and 20 mL methanol were added. The solution was left stirring for 2 days, and 40 mL ethanolamine was then added. The temperature was elevated to 80 °C to allow a less viscous environment. After 10 min, the brown solution changed into a brown-red-wine-like color. The solution was stirred for an additional 1 h and then the heating and stirring turned off and the solution left untouched for the weekend. After the weekend a solid brown crust layer appeared above the red-wine-like colored ethanolamine solution. The brown solid crust was filtered under vacuum and washed with acetonitrile (2×20 mL), methanol (1×10 mL) and diethyl ether (3×5 mL). After the washing with diethyl ether, the cluster changed from dark brown to greenish. Yield: 9.23%. The solid was analyzed as $[Mn_{12}O_{12}(O_2CC_4H_8N)_{16}(H_2O)_4] \cdot 1MeCN \cdot 5MeOH \cdot 5ETA \cdot 12EtOH$. Anal. Calcd for $C_{121}H_{266}N_{22}Mn_{12}O_{62}$: C, 38.157; H, 7.039; N, 8.09%. Found: C, 38.195; H, 6.964; N, 8.037%. FTIR: $\nu = 715\text{--}500$ (s, Mn-O), 1300–1900 (s, C=O), 1650 (s, in-plane N-H deformations),

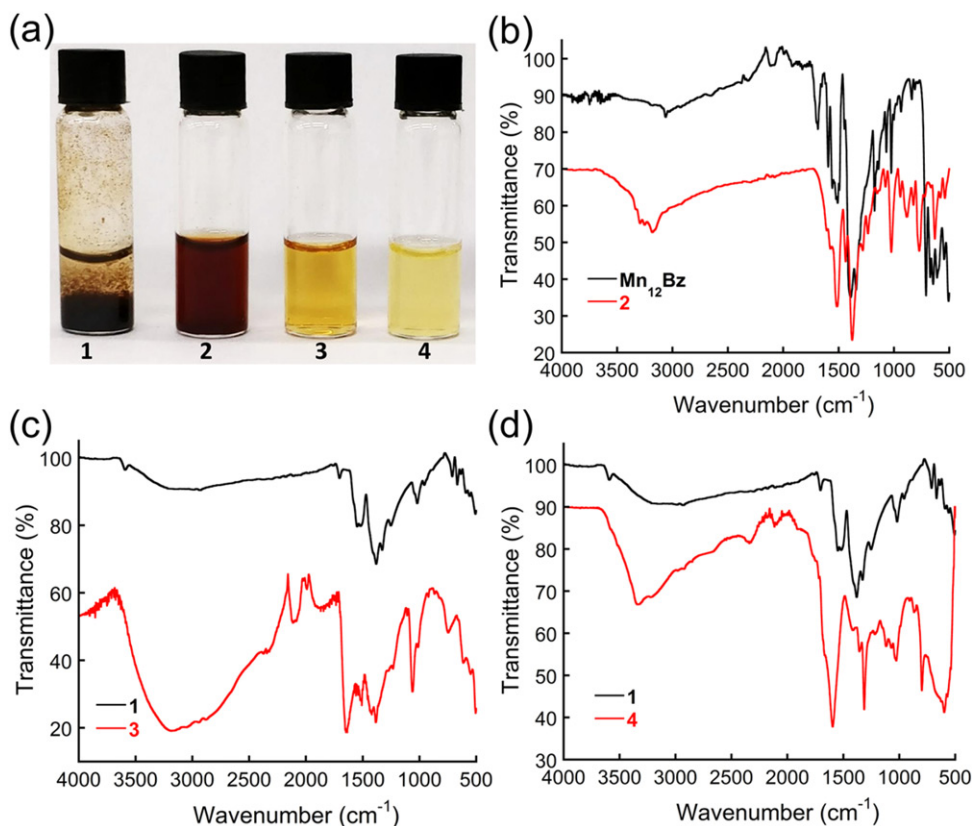


Figure 3. (a) Vials containing the clusters 1–4 in water; (b)–(d) FTIR spectra of 2, 3, and 4, respectively, compared to the spectra of $[\text{Mn}_{12}\text{O}_{12}(\text{O}_2\text{CPh})_{16}(\text{H}_2\text{O})_4]$ (Mn_{12}Bz) or 1.

2900–3200 (bs, intermolecular N-H), 3000 (m, stretching mode of N-H) cm^{-1} . MS (ESI-MS) m/z : Calcd (for $[\text{Mn}_{12}\text{O}_{12}(\text{O}_2\text{CC}_4\text{H}_8\text{N})_{16}(\text{H}_2\text{O})_4] \cdot 1\text{MeCN} \cdot 5\text{MeOH} \cdot 5\text{ETA} \cdot 12\text{EtOH}$): 3808.8; Found: 3054.7 ($[\text{Mn}_{12}\text{O}_{12}(\text{O}_2\text{CC}_4\text{H}_8\text{N})_{16}(\text{H}_2\text{O})_4] \cdot 5\text{ETA}$).

2.3.4. Synthesis of $[\text{Mn}_{12}\text{O}_{12}(\text{O}_2\text{CC}_5\text{H}_8\text{O}_4)_{16}(\text{H}_2\text{O})_4]$ (**4**)

To a stirred dark brown solution of $1 \cdot 2\text{MeCO}_2\text{H} \cdot 4\text{H}_2\text{O}$ (0.50 g, 0.24 mmol) in acetonitrile (40 mL), white L-ascorbic acid (1.70 g, 9.66 mmol) was added as a solid. Ethanol (100 mL) was then added in order to improve the ligand solubility, and the color changed to grayish–brown. The temperature was elevated to 85°C for 3 h in order to further drive the endothermic reaction. After 3 h, the solution became gray and the heating was turned off (slow cooling to r.t.). The solution was kept under continuous stirring for 3 days, and the color was then yellow (opaque). The solution was then filtered under vacuum, washed with acetonitrile (15 mL), ethanol (2×20 mL), methanol (10 mL) and diethyl ether (2×20 mL), and dried. Yield: 65.583% (on the basis of **1**). The solid was analyzed as $[\text{Mn}_{12}\text{O}_{12}(\text{O}_2\text{CCH}_3)_{14}(\text{C}_6\text{H}_6\text{O}_6)_2 \cdot (\text{H}_2\text{O})_4] \cdot 9\text{H}_2\text{O}$. *Anal.* Calcd for $\text{C}_{40}\text{H}_{80}\text{Mn}_{12}\text{O}_6$: C, 21.256%; H, 3.567%. Found: C, 21.258%; H, 3.30%. FTIR: $\nu = 715\text{--}500$ (m, Mn–O), 1090–1140 (m, –OH), 1300–1600 (s, C=O) 3200–3600 (broad, strong

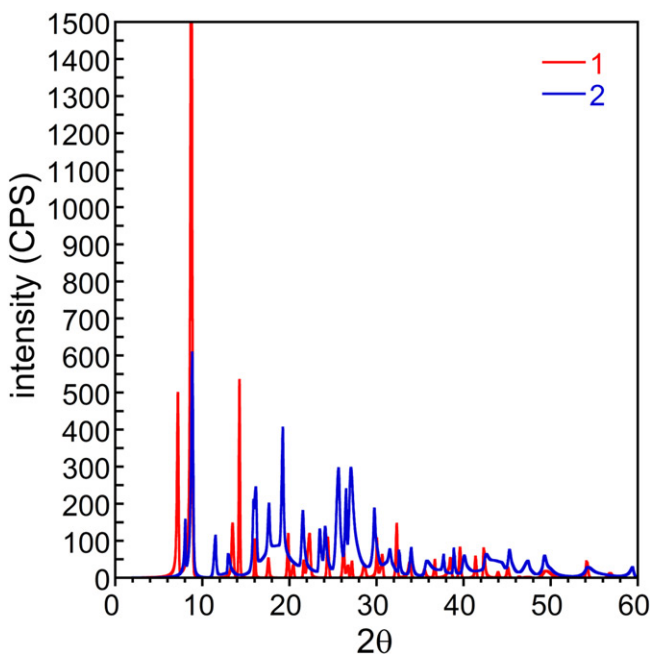


Figure 4. Powder X-ray diffraction patterns within the range of 2θ ($0\text{--}60^\circ$) for **2**, compared to **1**.

doublet band, two O-H groups stretching) cm^{-1} . MS (ESI-MS) m/z : Calcd (for $[\text{Mn}_{12}\text{O}_{12}(\text{O}_2\text{CCH}_3)_{14}(\text{C}_6\text{H}_6\text{O}_6)_2 \cdot (\text{H}_2\text{O})_4] \cdot 9\text{H}_2\text{O}$): 2259.56; Found: 2259.2. Powder XRD, 2θ values of selected peaks: 11.60, 16.01, 17.18, 18.49, 19.03 (100% intensity), 20.79, 22.70, 24.57, 26.35, 27.19, 29.68, 31.20, 32.11, 33.82, 38.59, 39.62, 42.23, 49.73, 54.19° .

3. Results and discussion

3.1. Synthesis and characterization of **2** and **3**

The clusters $[\text{Mn}_{12}\text{O}_{12}(\text{dab})_{16}(\text{H}_2\text{O})_4]$ (**2**) and $[\text{Mn}_{12}\text{O}_{12}(\text{pro})_{16}(\text{H}_2\text{O})_4]$ (**3**) were prepared by treatment of **1** with 40 equiv. of dabH or proH in acetonitrile, with the addition of acetone or ethanolamine, respectively, in order to increase the solubility of the hydrophilic ligands in the organic media (Equation (1)) [7]. The reaction mixtures with dabH and proH were stirred for 2 days, followed by heating the solution mixture at 80°C in the case of proH. The products **2** and **3** precipitated over a period of 1–2 days from the reaction solution as red-brown and green-brown solids, respectively, were collected, washed, and dried. The dry solid powders were very soluble in water giving clear brown solutions (Figure 3a) with no flocculants or precipitation, remaining clear for long periods (months). The two clusters were characterized by elemental analysis together with FTIR, UV-Vis and XPS spectroscopies, MS, and powder XRD analysis. The characterization data of the complexes are consistent with the assigned formula from the elemental analysis measurements as detailed in the Experimental section.

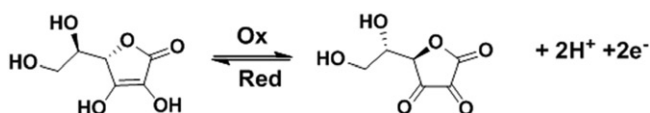
The FTIR spectrum of **2** is compared in Figure 3b to the FTIR spectra of $[\text{Mn}_{12}\text{O}_{12}(\text{O}_2\text{CPh})_{16}(\text{H}_2\text{O})_4]$ (**Mn₁₂Bz**) [7]. The two spectra have similar peak patterns, slightly shifted (for example 711 cm^{-1} , assigned to 5-adjacent-aromatic C-H, is shifted to 775 cm^{-1} ,

assigned to 2-adjacent-aromatic C-H). Furthermore, the spectrum of **2** includes the following additional bands: (i) a broad band at 3100–3350 cm⁻¹ assigned to N-H stretch of the primary amine, which is very intense due to an extensive hydrogen-bond network, (ii) primary amine N-H deformation bands at 1260–1440 cm⁻¹, (iii) aromatic C-N stretching at 1200–1390 cm⁻¹, (iv) *meta-para*-diamine di substituted benzene bands at 690–820 cm⁻¹, and (v) N-H wag band at 910–665 cm⁻¹. In comparison between the FTIR spectra of **Mn₁₂Bz** and **2**, it can be determined that the [Mn₁₂O₁₂(O₂CR)₁₆(H₂O)₄] structure was not damaged due to the employed conditions of carboxylate substitution, as the spectra are comparable [7]. This was further supported by the XPS spectrum of **2**, which is similar to that of **1** [8], exhibiting two typical Mn-O peaks (supporting information Figure S1). Additionally, the UV-Vis spectrum of **2** in water shows two absorption bands near 264 nm and 300 nm, which are about 3 nm shifted, in comparison to the free dabH (supporting information Figure S2). The structure was verified by MS analysis (supporting information Figure S3), showing the mass of the cluster with eight hydrate water molecules – [Mn₁₂O₁₂(O₂CC₆H₃(NH₂)₂)₁₆(H₂O)₄]·8H₂O at 3484.2 m/z. The powder XRD spectrum of **2**, compared to **1** (Figure 4), showed that the diffraction pattern was preserved, however with slight deviations resulting from wider packing, due to the bulky residues: the main diffraction peak appears at 2θ value of 8.84° (100%) compared to 8.73° for **1**; some of the peaks are slightly shifted to lower 2θ due to bulkiness of the residues. Overall, the combined data confirm that **2** is a new member of the Mn₁₂ family.

From comparison between the FTIR spectra of **3** and **1** (Figure 3c), it is clear that they both have the same Mn-μ-oxo bands at 715–500 cm⁻¹ and carbonyl bands at 1300–1900 cm⁻¹. In addition, **3** has several characteristic bands, amine N-H deformation at 1650 cm⁻¹ and an intense broad absorbance band near 3000 cm⁻¹, which corresponds to the secondary amine. The FTIR spectra suggests that **3** also retains the [Mn₁₂O₁₂(O₂CR)₁₆(H₂O)₄] structure. This is further confirmed by XPS measurements of **3**, which show two typical Mn peaks, with binding energy of 657.2 eV and 645.5 eV, corresponding to Mn^{III} and Mn^{IV}, respectively (supporting information Figure S4). The smooth shape of the peaks may reflect the presence of Mn^{III}, which is more dominant in comparison to Mn^{IV} in this cluster [9]. The UV-Vis spectra of both **1** in methanol and proH in water do not show absorbance in the UV-Vis region (supporting information Figure S5), but the spectrum of **3** (supporting information Figure S5) shows a peak at 327 nm, which can be assigned to the cluster formation. The structure was verified by MS analysis (supporting information Figure S6), showing the mass of the cluster with five ethanolamine molecules as solvates – [Mn₁₂O₁₂(O₂CC₄H₈N)₁₆(H₂O)₄]·5ETA at 3054.7 m/z. The powder XRD spectrum of **3** (supporting information Figure S7) presents amorphous structure, without any distinct diffraction peaks, and therefore is inconclusive for structure determination. This may result from the intensive hydrogen bonding involved with the material. Overall, this combined data suggest that **3** is a new Mn₁₂ cluster.

3.2. Synthesis and characterization of **4**

Cluster **4** was prepared by treatment of **1** with 40 equiv. of asCH ligand in acetonitrile, with the addition of ethanol in order to increase the solubility of the hydrophilic ligands in the organic media (Equation (1)). The reaction mixture was stirred at 85 °C



Scheme 1. L-ascorbic acid (left) oxidation to L-dehydroascorbate (right).

for 3 h followed by slow cooling to r.t. in which the reaction mixture was kept under continuous stirring for 3 days. Over this time, the product precipitated from the reaction solution as a yellow solid, was collected, washed, and dried. The dry solid powder was obtained in a moderate yield of 66% and most importantly was highly soluble in water with no flocculants or precipitating residues. The color of this solution, however, was very light brown, actually rather yellow. The characteristic color of Mn₁₂ clusters in water (or for these which do not dissolve in water, in any organic solvent) is dark brown, which is assigned to the Mn^{III} and Mn^{IV} oxidation states. Therefore, the solution color of **4** suggests that it is not a typical member of the Mn₁₂ family.

L-Ascorbic acid (vitamin C) is considered to be a “redox non-innocent” ligand [10]. This molecule is an “antioxidant” in nature and acts as a reducing agent; it can undergo two-electron oxidation to form L-dehydroascorbate (Scheme 1).

The FTIR spectrum of ascH (supporting information Figure S8a) verifies that it is indeed in its reduced form [11] (Scheme 1, left). The FTIR spectrum of **4**, however, implies that within the cluster, the ligand is in its oxidized form [11] (Scheme 1, right), as three major characteristic peaks are present: the stretching bands of the two O-H groups between about 3200–3600 cm⁻¹ and the two carbonyl peaks near 1400 and 1550 cm⁻¹ (supporting information Figure S8b) [11]. This indicates that the ascH ligands are oxidized during the carboxylate ligand substitution reaction, suggesting that one or more manganese ions are reduced by the ligand during this reaction. Another important observation from the comparison between the FTIR spectra of **1** and **4** (Figure 3d) is that the typical “finger print” bands at $\nu = 500\text{--}715\text{ cm}^{-1}$, which correspond to the Mn- μ -O core of Mn₁₂ clusters, have changed and broaden. This is probably due to the decrease in these bonds and the presence of Mn^{II}-OH bond stretches, which take place $>400\text{ cm}^{-1}$ (see supporting information Figures S9 and S10). This important observation, together with the ligand oxidation, and the yellow color of the cluster, supports the idea that the inorganic core underwent reduction by the ligand during the synthesis such that some of the manganese ions present in the cluster are in the Mn^{II} oxidation state.

In order to further examine the oxidation states present in **4**, XPS measurements were performed, showing two main types of Mn peaks with binding energy of 653.4 eV and 665.1 eV, corresponding to Mn^{III} and Mn^{IV}, respectively, and a small band at 658 eV, indicating the presence of Mn^{II} ions (supporting information Figure S11). ICP measurements were performed to quantify the number of manganese ions in the cluster (see Experimental section for details). The results indicate the presence of 1.758 mg/L of Mn in the solution, and the calculated fraction of the metal in the cluster correlated with 12 manganese ions. The UV-Vis spectrum of the ascH in water shows an absorbance at 265 nm (supporting information Figure S12, blue) and the spectrum of **4** in water (supporting information Figure S12, red) shows two peaks, a peak at 262 nm, which corresponds to asc (slightly blue shifted), and a peak at

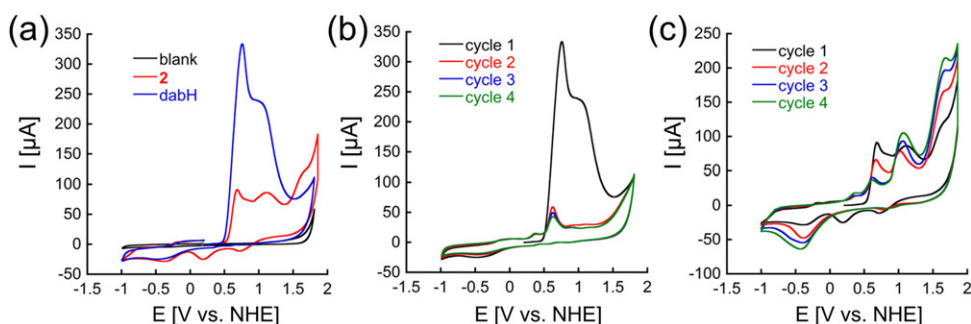


Figure 5. (a) Cyclic voltammograms of 0.1 M acetate buffer solutions of **2** (red), dabH (blue) and the blank (black) at pH 6. (b)–(c) Four continuous CV scans of 0.1 M acetate buffer solutions of dabH and **2**, respectively, at pH 6. CV scans were in the anodic direction.

348 nm, which can be assigned to the cluster formation. Collectively these results support the formation of a reduced Mn_{12} cluster, which contains three types of manganese ions, Mn^{II} , Mn^{III} , and Mn^{IV} . The elemental analysis results indicated only a partial substitution of acetate by asc ligands. The composition which best matched the found carbon and hydrogen weights is $[Mn_{12}O_{12}(O_2CCH_3)_{14}(C_6H_6O_6)_2 \cdot (H_2O)_4] \cdot 9H_2O$, in which only two asc ligands in their "dehydro" form, along with fourteen acetate ligands, are present in the organic shell. MS analysis (supporting information Figure S13) further supports the formation of this cluster showing the exact mass of this cluster at 2259.2 m/z. From these results, we cannot determine which two acetates have been replaced but there have been reports in the literature showing that the carboxylate ligands of Mn_{12} clusters may undergo partial site-selective substitution with preference for the axial position ("type A carboxylates") [12]. Taking into account that ascH is a cyclic molecule, which cannot form the typical $Mn-O(\mu_2-\eta^3\text{-acetate})$ bond, the substitution reaction should be difficult despite its low pKa. This could explain the partial ligand exchange that leads to the formation of **4**. In addition, powder XRD of **4** (supporting information Figure S14) suggests the cluster did not retain the classical Mn_{12} pattern, although some diffraction peaks overlap. The main diffraction peak at 2θ of 8.73° is absent. Therefore, in the lack of crystals suitable for X-ray analysis, the structure of **4** could not be confirmed.

3.3. Electrochemical investigations of **2**

The cyclic voltammetry (CV) chromatograms of dabH and **2** were recorded at pH 6 in acetate buffer after purging with a N_2 stream to eliminate residuals of dissolved oxygen (Figure 5a). Cluster **2** in this medium scanning initially in the anodic direction displays three oxidation waves at $E_p = 0.65$ V, 1.2 V, and 1.55 V versus NHE, and three cathodic peaks at $E_p = 0.75$ V, 0.2 V, and -0.45 V versus NHE (Figure 5a, red line). Under the same conditions, dabH exhibited two irreversible oxidation peaks at 0.65 V and 1.1 V versus NHE (Figure 5a, blue line). Thus, the first oxidation peak of **2** is assigned to the ligand irreversible oxidation, the second oxidation peak can be

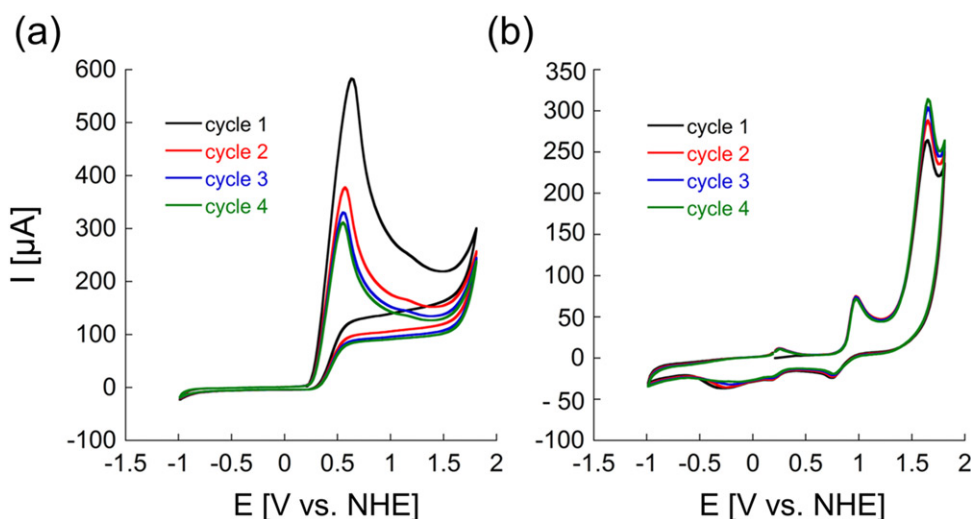


Figure 6. Four continuous CV scans of 0.1 M acetate buffer solutions containing asCH (a) and **4** (b), respectively, at pH 6. CV scans were in the anodic direction.

considered as an overlapping of two peaks: Mn^{III} to Mn^{IV} oxidation and dabH oxidation peak, originally at 1.1 V. The third peak (poorly resolved) is assigned to a second Mn^{III} to Mn^{IV} oxidation. At the cathodic side, the first reduction peak is assigned to the second $\text{Mn}^{\text{IV/III}}$ reduction and the second reduction peak is assigned to the first $\text{Mn}^{\text{III/IV}}$ reduction (see Figures 1b and 2b in Ref. 6). The third reduction peak (small) appears at -0.45 V and is assigned to molecular oxygen reduction [13].

Continuous CV scans of four cycles were conducted to the free dabH (Figure 5b), and to **2** (Figure 5c) at pH 6. The ligand undergoes irreversible oxidation, and after the first cycle, the peaks at 0.65 V and 1.1 V versus NHE decrease, and a new small peak appears at 0.39 V versus NHE. The cluster has an unstable redox pattern, and the CV changes with the cycles: following the first cycle, the intensity of the peaks corresponding to the oxidation of dab is decreased, because the ligand is already in its oxidized state, and the intensity of the waves related to $\text{Mn}^{\text{III/IV}}$ oxidation increase because (as dab is already oxidized) the supplied charge is “available” to oxidize the manganese ion. The oxygen reduction peak is increasing implying that oxygen is evolved, probably due to some catalytic water oxidation process, which is possible when greater amount of high-oxidation-state Mn ions became available in the solution. Despite this observation, we conclude that **2** does not hold potential as a water oxidation electrocatalyst due to its instability during the electrochemical redox process, which is a consequence of: (i) the immediate oxidation of dab resulting in a cluster different than **2** that is not water-soluble and eventually precipitates and (ii) the reduction of one of the Mn^{III} ions that also changes the cluster.

3.4. Electrochemical investigations of **3**

The CV of **3** was recorded at pH 6 in acetate buffer, which was purged with a N_2 stream prior to the measurements (supporting information Figure S15). The CV of

proH has an oxidative catalytic peak, as can be seen at potentials of +1.2 V versus NHE and beyond, which can arise from either ligand oxidation and/or water oxidation. As there is no detected oxygen reduction peak, we assume that this is the oxidation of the secondary amine. The CV of **3** exhibits two oxidation waves at $E_p = 0.78$ V and 1.5 V versus NHE (very small and poorly resolved) before the solvent oxidation peak and two reduction peaks at $E_p = 0.5$ V and -0.5 V versus NHE. The first (sharp) oxidation wave can be assigned to Mn^{III} to Mn^{IV} oxidation and the second one (very small and poorly resolved shoulder) can be assigned to the second Mn^{III} to Mn^{IV} oxidation. The first reduction peak can be assigned to Mn^{IV} to Mn^{III} reduction and the second reduction peak at -0.5 V is assigned to molecular oxygen reduction. The unique shape of this cluster, in comparison to other water soluble Mn_{12} clusters like **Mn₁₂DH**, **2** and **4** (see below), and the similarity in current intensity of the water oxidation peak with or without the cluster (about 90 μ A and 50 μ A, respectively), suggest that this cluster is also not a potential water oxidation electrocatalyst.

3.5. Electrochemical investigations of **4**

Continuous CV scans of four cycles were conducted for free asCH (Figure 6a) and for **4** (Figure 6b) at pH 6. The ligand undergoes oxidation to the dehydroascorbate form, and the intensity of the oxidation peak near 0.5 V versus NHE decreases with the cycles, respectively. The CV of the cluster exhibits three oxidation peaks at $E_p = 0.25$ V (small) assigned to Mn^{II} to Mn^{III} oxidation, 0.95 V (intense, about 90 μ A) assigned to Mn^{III} to Mn^{IV} oxidation, and 1.5 V versus NHE (very intense, about 300 μ A), which is assigned to the second Mn^{III} to Mn^{IV} oxidation. The cluster exhibits three reduction peaks at $E_p = 0.75$ V, which can be assigned to Mn^{IV} to Mn^{III} reduction, 0.25 V (small) that can be assigned to Mn^{III} to Mn^{II} reduction, and -0.6 V (small) that can be assigned to the reduction of molecular oxygen. From the continuous CV scan experiments showing that the peak shape and intensity are constant throughout the cycles, it is evident that **4** is stable toward electrochemical oxidation reaction, suggesting that the cluster retains its structure during the reversible redox process. Moreover, this CV resembles the CV chromatograms of **2** and **Mn₁₂DH** measured in the same concentration and reaction conditions, supporting the assumption that it is a Mn_{12} cluster, only reduced, as was suggested by the ICP analysis. The low intensity of the oxygen reduction peak, which does not increase with the cycles, implies, however, that there is no oxygen evolution in this process and therefore no catalytic water oxidation occurs, probably because the Mn ions responsible for this catalytic process are in their reduced Mn^{II} form in this cluster and thus cannot oxidize water.

4. Conclusions

This work describes the challenges in generating water-soluble and stable Mn_{12} clusters as potential oxidation catalysts. Three such clusters, **2**, **3**, and **4**, were synthesized via substitution of the acetate ligand in **1** by dab, pro or asc ligands, respectively, characterized by various spectroscopic techniques and their electrochemical performances in water were examined. Based on elemental analysis, UV-Vis and FTIR

spectroscopies, XPS, MS and powder XRD analyses, we suggest that **2** and **3** might be new members of the Mn_{12} family and **4** might be a partially substituted reduced Mn_{12} cluster. Electrochemical measurements at pH 6 support the proposed structures and imply that: (i) while **2** exhibits some water oxidation activity, it is unstable toward the oxidation process because the primary amine ligands are oxidized rapidly and (ii) although **3** and **4** do not show water oxidation activity, **4** remains stable throughout the oxidation process. In all cases, it is suggested that these clusters cannot serve as electrocatalysts for water oxidation; however, the high stability of **4** makes it a potential catalyst for other oxidation reactions [14], and future studies should initially focus on obtaining single crystals suitable for X-ray analysis that will provide its high-resolution structural characterization. Cluster **3** includes proline, which is an excellent catalyst for various transformations [15, 16], specifically for carbon-carbon bond forming reactions [17, 18], and its combination with high-oxidation manganese ions within this cluster might lead to the ability of **3** to act as a bifunctional catalyst for a variety of processes other than water oxidation. Furthermore, the high water solubility of these clusters should provide access to their use in water as an inexpensive and “green” solvent.

Acknowledgements

The authors thank Dr. Kamira Weinfeld from the Surface Science Laboratory Solid State Institute at the Technion for the XPS measurements and Dr. Maria Koifman from Wolfson center for interface science at the Faculty of Science and Materials Engineering, Technion for the powder XRD measurements. G. M. thanks Prof. George Christou for fruitful discussions and for the picture of **1** in the graphical abstract figure.

Disclosure statement

No potential conflict of interest was reported by the authors.

Funding

This research was funded by the Solar Fuels Israel Center of Research Excellence (I-CORE) of the Israeli Science Foundation (ISF), grant number 2018762, and supported by the Grand Energy Technion Program.

ORCID

Galia Maayan  <http://orcid.org/0000-0001-5711-7339>

References

- [1] R. Bagai, G. Christou. *Chem. Soc. Rev.*, **38**, 1011 (2009).
- [2] S. Mukherjee, J.A. Stull, J. Yano, T.C. Stamatatos, K. Pringouri, T.A. Stich, K.A. Abboud, R.D. Britt, V.K. Yachandra, G. Christou. *Proc. Natl. Acad. Sci. U.S.A.*, **109**, 2257 (2012).
- [3] M. Soler, W. Wernsdorfer, K.A. Abboud, J.C. Huffman, E.R. Davidson, D.N. Hendrickson, G. Christou. *J. Am. Chem. Soc.*, **125**, 3576 (2003).

- [4] T. Lis. *Acta. Crystallogr., Sect. B*, **36**, 2042 (1980).
- [5] Y. Yan, J.S. Lee, D.A. Ruddy. *Inorg. Chem.*, **54**, 4550 (2015).
- [6] G. Maayan, N. Gluz, G. Christou. *Nat. Catal.*, **1**, 48 (2018).
- [7] R. Sessoli, H.L. Tsai, A.R. Schake, S. Wang, J.B. Vincent, K. Folting, D. Gatteschi, G. Christou, D.N. Hendrickson. *J. Am. Chem. Soc.*, **115**, 1804 (1993).
- [8] J. Means, V. Meenakshi, R.V.A. Srivastava, W. Teizer, A.I.A. Kolomenskii, H.A. Schuessler, H. Zhao, K.R. Dunbar. *J. Magn. Magn. Mater.*, **284**, 215 (2004).
- [9] A number of studies modeled Mn2p_{3/2} spectral components in XPS for characterizing the Mn(II), Mn(III), and Mn(IV) oxidation states according to their multiplet splitting and their peaks shapes, for example: (a) H.W. Nesbitt, D. Banerjee. *American Mineralogist*, **83**, 305 (1998); (b) E.S. Ilton, J.E. Post, P.J. Heaney, F.T. Ling, S.N. Kerisit. *Appl. Surf. Sci.*, **366**, 475 (2016).
- [10] W. Kaim, B. Schwederski. *Coord. Chem. Rev.*, **254**, 1580 (2010).
- [11] S. Kinugasa, K. Tanabe, T. Tamura, *SDBS - Spectral Database for Organic Compounds*, National Institute of Advanced Industrial Science and Technology (AIST), Japan (2018).
- [12] P. Artus, C. Boskovic, J. Yoo, W.E. Streib, L.-C. Brunel, D.N. Hendrickson, G. Christou. *Inorg. Chem.*, **40**, 4199 (2001).
- [13] C. Song, J. Zhang, In *PEM Fuel Cell Electrocatalysts and Catalyst Layers: Fundamentals and Applications*. Chap. 2, pp. 89–134. ISBN 978-1-84800-936-3.
- [14] G. Maayan, G. Christou. *Inorg. Chem.*, **50**, 7015 (2011).
- [15] D.B. Ramachary, N.D. Chowdari, C. Barbas. *Tetrahedron Lett.*, **43**, 6743 (2002).
- [16] N. Vignola, B. List. *J. Am. Chem. Soc.*, **126**, 450 (2003).
- [17] B. List, R.A. Lerner, C.F. Barbas. *J. Am. Chem. Soc.*, **122**, 2395 (2000).
- [18] B. List, P. Pojarliev, W.T. Biller, H.J. Martin. *J. Am. Chem. Soc.*, **124**, 827 (2002).